SCIEPublish

Article

Optimization of Powder Distribution and Feeding Efficiency Using an Annular Powder-Feeding Nozzle: A Numerical and Experimental Study

Md Shahriar Islam, Deping Yu *, Jier Qiu, Yu Xiao and Ying Fan

School of Mechanical Engineering, Sichuan University, Chengdu 610065, China; shahriar.islam.saykot@gmail.com (M.S.I.); 604127403@qq.com (J.Q.); 15848349306@163.com (Y.X.); 2035179526@qq.com (Y.F.)

* Corresponding author. E-mail: williamydp@scu.edu.cn (D.Y.)

Received: 13 April 2025; Accepted: 16 June 2025; Available online: 20 June 2025

ABSTRACT: The quality of spherical powders required in plasma spheroidization is particularly important to advanced manufacturing, such as additive manufacturing and thermal spray coatings. Traditional powder feeding systems, such as radial and coaxial nozzles, often suffer from suboptimal powder distribution, low powder capture efficiency, and poor control of particle trajectories. These issues deteriorate spheroidization quality and material efficiency. We propose here an innovative annular powder-feeding plasma torch for these challenges and to optimize the powder-feeding dynamics. The novel nozzle consists of a tangential powder feeding mechanism and a concentric conical structure that provides uniform powder distribution and minimizes plasma jet interference. Computational fluid dynamics (CFD) simulations and Discrete Phase Modeling (DPM), combined with a literature review, are used to study such as throat size and convergent-divergent profiles of nozzles for gas-powder interactions. Yttria-Stabilized Zirconia (YSZ) powder was used for the experimental validation of the annular nozzle; the annular nozzle was found to outperform traditional nozzles in this application with a powder capture efficiency of 75%, a deposition efficiency of 92%, and a spheroidization efficiency of 85%; 85% of the particles had a circularity index >0.9. These results indicate that powder distribution uniformity, deposition efficiency, as well as spheroidization quality are greatly improved than those from conventional plasma spheroidization systems, demonstrating the potential for better process performance for plasma spheroidization. These findings demonstrate the relevance of the optimized annular nozzle in the field of high-value material manufacturing as it yields increased coating quality and minimized material wastage.

Keywords: Arc plasma torch; Plasma spheroidization; Annular powder feeding; Computational fluid dynamics; DPM simulation

1. Introduction

Plasma spheroidization is a crucial process in advanced material manufacturing, particularly for producing high-quality spherical powders used in additive manufacturing and other high-performance applications [1,2]. The process involves injecting powder particles into a high-temperature plasma jet, melting, and spheroidized them before solidifying them into spherical particles with uniform size and morphology [3,4]. The quality of spheroidized powders is highly dependent on powder feeding efficiency and particle distribution uniformity within the plasma jet [5,6]. However, conventional powder-feeding systems, such as radial and coaxial nozzles, often suffer from uneven powder distribution, low powder capture efficiency, and inadequate control over particle trajectories, leading to suboptimal spheroidization quality and material wastage [7,8].

Recent advancements in plasma spheroidization have highlighted the importance of nozzle geometry and gas-powder dynamics in achieving uniform powder distribution and high spheroidization efficiency. Annular powder-feeding nozzles have emerged as a promising solution, offering superior powder convergence and concentration compared to traditional designs [9]. Annular nozzles have been shown to achieve a powder capture efficiency of 75%, significantly outperforming discrete three-outlet nozzles [10]. This breakthrough underscores the potential of annular nozzles

https://doi.org/10.70322/htm.2025.10015

to optimize powder usage rates and enhance spheroidization quality [11]. However, challenges such as uneven powder flow, nozzle clogging, and inadequate heat dissipation persist, necessitating further innovation in nozzle design [12,13].

Although progress has been made in nozzle design, current annular powder feeding systems have some serious limitations [14,15]. For instance, powder flow is uneven, and inflow and outflow can be turbulent inside the nozzle, resulting in material loss and inconsistent spheroidization quality. Furthermore, conventional designs fail to maintain efficient powder convergence and heat dissipation, which are both of extreme importance for high spheroidization rate and homogeneous particle morphology. These limitations highlight the need for next-generation annular powder-feeding nozzles that integrate advanced feeding mechanisms and undergo rigorous experimental validation [16].

The use of gas discharge to obtain spherical particles is a well-established technique that has been known for the last century. Early foundational work laid the groundwork for modern plasma spheroidization techniques, demonstrating the potential of gas discharge methods for producing high-quality spherical powders with uniform size and morphology [17]. More recent advancements in plasma technology have further optimized these processes, allowing for precise control over particle size and shape. Various plasma conditions have been explored, highlighting the importance of optimizing parameters such as gas flow rate, plasma power, and powder feed rate to achieve desired particle characteristics [18]. In addition to optimizing the powder-feeding nozzle design, understanding the properties of the powders before and after plasma treatment is crucial for achieving high-quality spherical particles. The initial properties of the powders, such as particle size distribution, morphology, and chemical composition, significantly influence the spheroidization process. Similarly, the properties of the construction materials used in the feed device, such as thermal conductivity, high-temperature resistance, and mechanical strength, play a vital role in ensuring stable and efficient powder delivery. Understanding the heat exchange and friction within the system is also crucial for ensuring efficient flow rates and stable operation. Heat exchange and friction are directly related to the properties of the material and the flow parameters, and they play a significant role in the overall efficiency of plasma technologies [19]. Efficient flow dynamics ensure that the powder particles are uniformly distributed and adequately exposed to the high-temperature plasma jet, leading to complete melting and spheroidization. Understanding and optimizing these flow dynamics are essential for improving the overall efficiency of the spheroidization process.

While our study focuses on the optimization of powder feeding using a DC-arc plasma torch, it is important to note that RF (radio frequency) plasma generators are currently more widely used in plasma spheroidization processes [20]. RF plasma generators offer certain advantages, such as higher power efficiency and better control over plasma parameters, which make them suitable for a wide range of applications [21]. However, DC-arc plasma torches, like the one used in our study, provide unique benefits such as simpler design, lower cost, and ease of operation, making them a viable option for specific industrial applications [22]. Our work aims to enhance the performance of DC-arc plasma torches by optimizing the powder feeding system, thereby improving the overall efficiency and quality of the spheroidization process.

This study aims to optimize powder distribution in plasma spheroidization using an innovative annular powder-feeding plasma torch. The objectives include improving powder convergence and spheroidization efficiency by optimizing nozzle geometry, specifically the convergent-divergent profile and throat size. Advanced computational fluid dynamics (CFD) simulations and Discrete Phase Modeling (DPM) are used for numerical analysis, complemented by experimental validation, to provide insights into the relationship between powder transport and spheroidization dynamics. The findings have direct applications in additive manufacturing and other advanced manufacturing technologies.

2. Materials and Methods

2.1. Nozzle Design and Features

Plasma spheroidization is a critical advancement in powder processing and benefits from the capability to inject powders precisely, sustain the plasma flow, and transfer energy efficiently. Modern plasma torches are adopting the conventional design to the advanced high-power configuration, which can improve the uniformity of the powder distribution and the efficiency of the spheroidization. A 3D-modeled laboratory plasma torch with an innovative annular powder feeding system is shown in Figure 1 as a cross-sectional view.

A cascade-designed plasma torch provides enhanced operational stability compared to conventional self-generating gap-length plasma torches due to its higher voltage working condition. It enables an optimized electrode configuration that brings about superior axial symmetry of the plasma jet and, in turn, reduces the arc fluctuations and enhances the plasma stability. Moreover, the annular powder feeding mechanism distributes the powder to the plasma for uniform heating and reducing particle trajectory deviations. These enhancements enhance a spheroidization process

to one that is optimized concerning powder morphology control and material loss, serving the process well for industrial powder modification purposes.

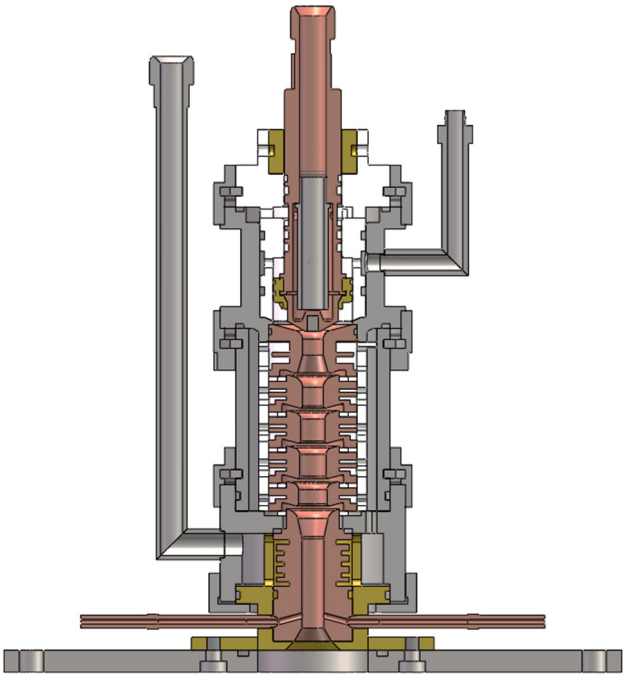

Figure 1. Cross-Sectional View of the IEI Plasma Torch with Annular Powder-Feeding System.

Radial Powder Feeding and Annular Powder-Feeding: A Dual-Mode Powder Injection System for Enhanced Coating Uniformity and Efficiency. The annular powder feeding nozzle is an innovative design that is designed to achieve the best powder distribution uniformity, greatly reduce plasma jet interference, and greatly improve the spheroidization efficiency. However, the novel nozzle is engineered in a very precise and detailed structure to ensure outstanding process control, precision, and performance, as evidenced by Figure 2.

The novel dual-mode injection system for enhanced coating uniformity and efficiency [23,24] uses distinct powder feeding mechanisms, as shown in Figure 2. The radial powder-feeding, which radially introduces the powder into the plasma jet, is shown in Figure 2a. This design usually gives a less controlled distribution of the powder, which in many cases produces uneven coating and lower spheroidization efficiency [25,26]. While some applications benefit from the radial injection system, challenges such as uniform powder flow and plasma jet interference ultimately limit overall performance in high-precision processes.

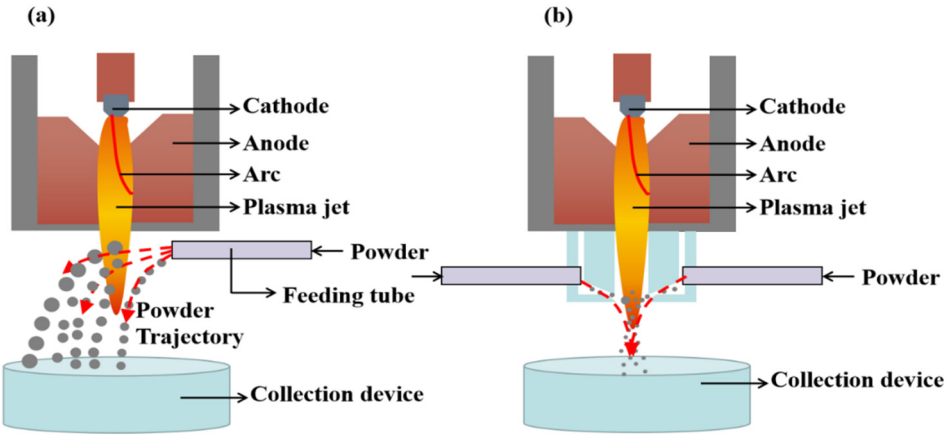

Figure 2. (**a**) Radial powder feeding, (**b**) Annular powder feeding.

Figure 2b shows the annular powder feeding nozzle, which is a major innovation in the plasma spheroidization field [27,28]. The power distribution uniformity and the process control are much improved than the previous nozzle design. The powder is injected through an annular ring to provide a more concentrated and uniform powder flow around

the circumference of the nozzle. Configuration of this configuration effectively eliminates the plasma jet interference by aligning the powder beam symmetrically with the plasma jet, which optimizes the spheroidization process. This dual-mode powder injection system used to obtain the result demonstrated the advanced capabilities of improved spheroidization efficiency and more consistent coating quality [29,30].

To unravel the intricacies of gas-powder dynamics within the nozzle, a sophisticated CFD-based two-phase flow model was developed, leveraging the structural insights from Figure 2. Utilizing the commercial software FLUENT 2021, comprehensive simulations were performed to scrutinize the nozzle's aerodynamic performance, encompassing pivotal aspects such as gas-powder interaction, particle trajectory mapping, concentration distribution analysis, and overall flow behavior [31].

As depicted in Figure 3a illustrates the overall design of the annular powder feeding nozzle, including the powder injection mechanism and the cooling scheme. The nozzle is designed to ensure uniform powder distribution and efficient heat dissipation. Figure 3b provides a detailed view of the multiple ring grooves, which are crucial for optimizing powder flow and distribution. The lower surface of this section is strategically outfitted with multiple ring grooves, including 28 specifically designed grooves that optimize powder entry into the channel [32]. This configuration ensures that the ejected powder beam remains symmetrically aligned with the plasma jet [33]. The design minimizes disturbances to the plasma flow while enhancing the uniformity of powder distribution. To further improve fabrication feasibility and thermal resistance, the minimum thickness of this section is maintained at ≥2 mm [34]. The primary function of the ring-groove section is to regulate the motion of powder particles, reduce their tangential velocity, and facilitate optimal powder convergence, which in turn promotes improved particle heating and spheroidization.

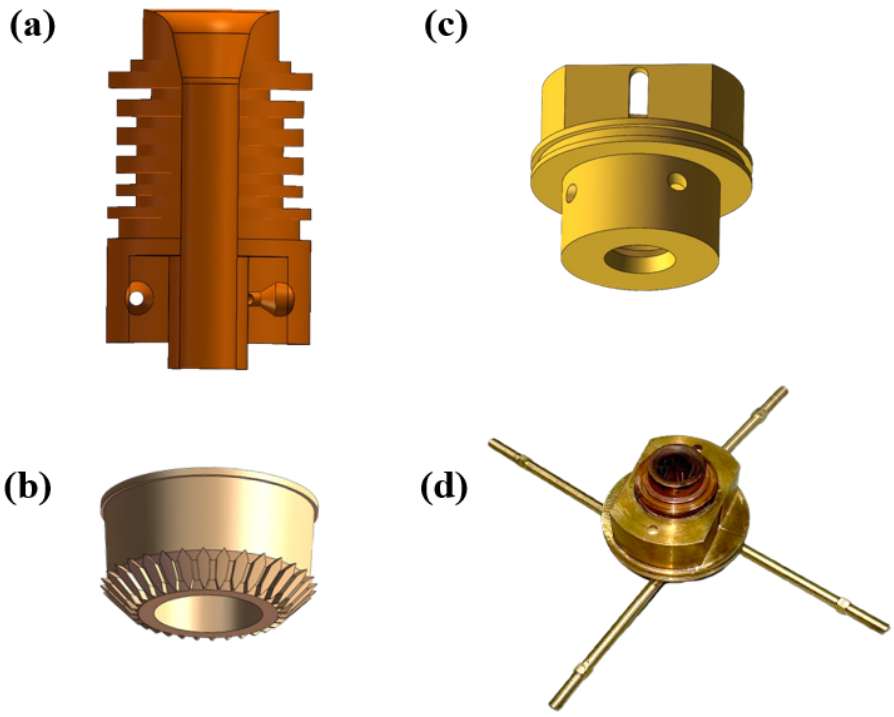

Figure 3. New-type Annular Nozzle. (**a**) Powder injection into the plasma and the cooling scheme; (**b**) Ring-groove section; (**c**) Nozzle tail and anode compression section; (**d**) Annular Plasma Nozzle Assembly.

The nozzle tail and anode compression section (Figure 3c) serve as the structural integration point for the entire nozzle assembly. This section, together with component Figure 3a, constitutes a convergent-divergent nozzle configuration that promotes plasma jet expansion and accelerates powder particles. This gives an advantage in the efficiency of spheroidization and in the overall powder processing performance. Finally, Figure 3d depicts the Integrated Annular Powder-Feeding Plasma Nozzle Assembly, which consists of the nozzle body, ring-groove section, and nozzle tail with anode compression. The spheroidization unit is an integrated structure that is carefully laid-out to maximize powder distribution, ensure a stable plasma jet, and maximize spheroidization efficiency by ensuring homogeneous particle injection and minimizing flow disturbance.

2.2. Assumptions

There are the following basic assumptions behind such analysis:

(1) Argon is taken as the continuous phase with constant density and viscosity throughout the process.
(2) The powder particle size distribution is the Rossin-Rammler distribution.
(3) It is assumed that the powder is uniformly distributed at the inlet, and the powder velocity is equal to that of the carrier gas.
(4) In the current analysis, the heat transfer due to plasma radiation on the powder particles is neglected.

2.3. Continuous Phase Model of Carrier Gas

The Navier-Stokes equations are solved to accurately capture the gas flow behavior in the newly designed annular powder feeding nozzle, which provides a complete mathematical framework [35]. Expressed in tensor form as follows, these equations form the foundation for simulating the complex gas dynamics within the nozzle's inner channel and outer jet structure, crucial for optimizing plasma spraying performance.

Mass Conservation Equation:

$$\frac{\partial(\rho_g u_{g,i})}{\partial x_i} + \frac{\partial(\rho_p u_{p,i})}{\partial x_i} = 0 \tag{1}$$

Momentum Conservation Equation:

$$\frac{\partial(\rho_g u_{g,i} u_{g,j})}{\partial x_i} + \frac{\partial(\rho_p u_{p,i} u_{p,j})}{\partial x_i} = -\frac{\partial p}{\partial x_i} + \frac{\partial}{\partial x_i}\left[(\mu_g + \mu_{g,t})\left(\frac{\partial u_{g,i}}{\partial x_j} + \frac{\partial u_{g,j}}{\partial x_i}\right)\right] + \rho g_i + F_{\text{drag}} \tag{2}$$

where the indices *i, j* = 1, 2, 3 take values of 1, 2, and 3, representing the components of the tenso; The terms u_i and g_i correspond to the components of the velocity vector and the gravitational acceleration vector, respectively. The variables ρ, ρ_g, t, μ and μ_t are gas density, pressure, time, molecular viscosity, and turbulent viscosity, respectively. Additionally, F_{drag} is the drag force due to gas-powder interaction. In this investigation, the gas density is considered constant due to the relatively low velocity and pressure drop [36]. The realizable $k-\varepsilon$ turbulence model enhances the traditional $k-\varepsilon$ model, facilitating computation [37].

The characterized of turbulent viscosity μ_t in this model by the following equation:

$$\mu_{g,t} = \rho_g C_\mu \frac{k^2}{\epsilon} \tag{3}$$

where C_μ denotes a variable that is derived from the field variables, developing it apart from the constant utilized in the traditional $k-\varepsilon$ model [38–40]. Here, k represents turbulent kinetic energy, whereas ε indicates the turbulent dissipation rate. The transport equations for k and ε are as follows:

$$\frac{\partial(\rho k u_j)}{\partial x_j} = \frac{\partial}{\partial x_j}\left[\left(\mu + \frac{\mu_t}{\sigma_k}\right)\frac{\partial k}{\partial x_j}\right] - \rho\overline{u_i' u_j'}\frac{\partial u_j}{\partial x_i} - \rho\epsilon + \mu_t^{\text{groove}} \tag{4}$$

$$\frac{\partial(\rho\epsilon u_j)}{\partial x_j} = \frac{\partial}{\partial x_j}\left[\left(\mu + \frac{\mu_t}{\sigma_\epsilon}\right)\frac{\partial \epsilon}{\partial x_j}\right] + \rho C_1 S\epsilon - \rho C_2 \frac{\epsilon^2}{k + k\sqrt{\nu\epsilon}} \tag{5}$$

where S represents the modulus of the mean strain rate tensor, which is defined as follows:

$$S^* = \sqrt{2\widetilde{S_{\iota J}}\widetilde{S_{\iota J}}\text{v}} \tag{6}$$

$$\widetilde{S_{\iota J}} = \frac{1}{2}\left(\frac{\partial \widetilde{u_\iota}}{\partial x_j} + \frac{\partial \widetilde{u_j}}{\partial x_i}\right) \tag{7}$$

C_1 is defined as:

$$C_1^* = \max\left(0.45, \frac{\zeta^*}{\zeta^* + 4.8}\right) \tag{8}$$

$$\zeta^* = \frac{S^* k}{\epsilon} \tag{9}$$

ν denotes the kinematic viscosity; C_1^* = 0.45 is the minimum value for the strain-to-dissipation ratio; C_2 = 1.9 is an actual constant; σ_k = 1.0 and σ_e = 1.2 are turbulent Prandtl numbers for *k* and ε, accordingly.

2.4. Dynamic Model of Powder Particles

Revolutionizing plasma spraying simulations, the model combines the two-way turbulence coupling model with the Discrete Phase Model (DPM) to capture the dynamic interplay between gas and powder particles. The dynamics of powder are analyzed by integrating the effects of resistance, inertia, and gravity. The trajectories of discrete particles in the Lagrangian coordinate system are determined by the following methodology:

$$\frac{dr_{p,i}}{dt} = u_{p,i} \tag{10}$$

$$\frac{du_{p,i}}{dt} = \frac{18\mu C_D Re}{\rho_p d_p^2 24}\left(u_i - u_{p,i}\right) + \frac{\left(\rho_p - \rho\right) g_i}{\rho_p} \tag{11}$$

where r_p, *i,* and up, accordingly *i* represent the axis vector and velocity vector of powder particles; ρ_p represents the density of the powder particles, while d_p denotes their diameter; the Reynolds number, denoted as Re, is a dimensionless quantity that characterizes the flow of fluid relative to a particle. It is defined as follows:

$$Re = \frac{\rho_p d_p \left|\mu_i - \mu_{p,i}\right|}{\mu} \tag{12}$$

The initial term on the right side of Equation (11) represents the resistance associated with each powder particle. C_D represents the drag value and the circular drag coefficient model is utilized in this structure [41,42]. The equation is as follows:

$$C_D = a_1 + \frac{a_2}{Re} + \frac{a_3}{Re^2} \tag{13}$$

where a_1, a_2 and a_3 represent actual variables.

During the gas-powder two-phase flow in the powder-feeding process of plasma spraying, the low volume fraction of powder leads to the disregard of particle collisions. The analysis is concentrated on the interactions between the powder particles and the surfaces of the cavity and nozzle. This model presumes a complete collision, with both normal and tangential recovery coefficients set at a value of 1 [38].

Stokes number (Stk) is an undefined quantity utilized to characterize the behavior of particles within the gas flow. It can be defined as follows [43]:

$$Stk = \frac{\rho_p d_p^2 Re}{18\rho L^2} \tag{14}$$

where the variable *L* represents the width of the powder flow channel within the nozzle. If the Stk of powder particles is significantly greater than 1 ($Stk \gg 1$), it indicates that turbulence can be disregarded due to the substantial weight of the powder particles. However, the influence of these particles on the gas flow field necessitates the implementation of a two-way turbulence coupling method. When $Stk \ll 1$ is much less than 1, it is essential to take into account the impact of turbulence on particles.

2.5. Boundary Condition

In this study, we consider a three-dimensional spatial flow for the gas-powder mixture within the nozzle, accounting for both axial and radial variations in the flow. The flow dynamics are simulated using a three-dimensional numerical model developed in FLUENT, as shown in Figure 4. The model simulates how the gas and powder interact along both the axis (length of the nozzle) and radius (across the nozzle's width), capturing the full distribution of powder particles. Additionally, volumetric flow refers to the overall flow rate and distribution of the gas-powder mixture, as modeled across the entire nozzle volume, including its axial and radial directions.

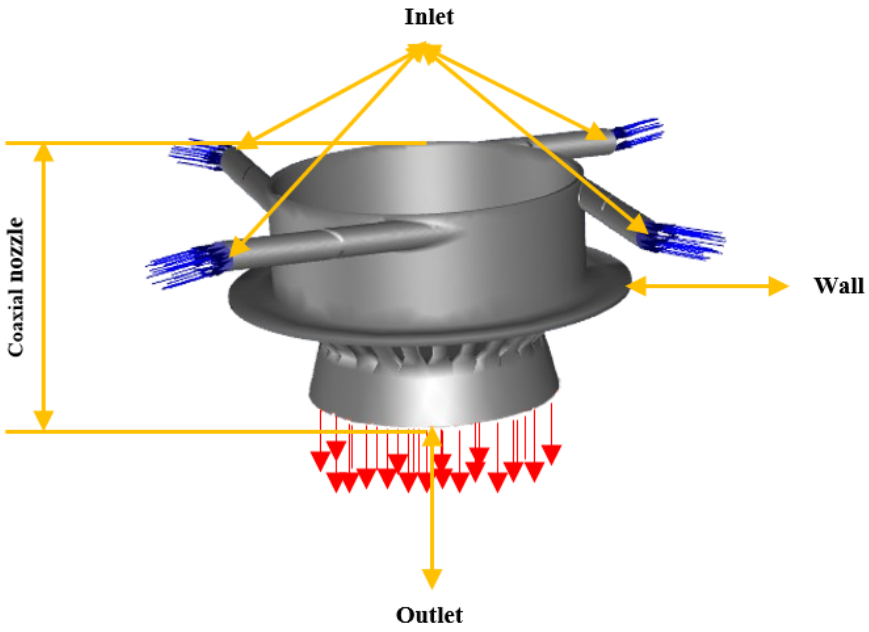

Figure 4. Computational domain.

This model only focuses on the flow of free powder, this model focuses only on the movement of free powder, creating a cylindrical calculation domain beneath the nozzle to explore the flow dynamics and convergence structure of the gas and powder jet flow in that area. The calculation domain of the upper part includes the inner flow channels within the mixing cavity of the nozzle, aimed at analyzing the flow characteristics of gas and powder that are difficult to observe through experimental methods. The initial conditions for the calculation are presented in Table 1, and the gas velocity V_{gas} can be approximately characterized as follows:

Table 1. Initial Boundary Conditions.

Boundary Condition Parameter	**Inlet Powder Feed Rate (g/min)**	**Outlet Carrier Gas Flow (L/min)**
Value	1.5	5
	2	8
	2.5	11
	3	17

The initial parameters for the calculation are presented in Table 1, and the gas velocity V_{gas} can be approximately characterized as follows:

$$V_{\text{gas}} = \frac{Q_{\text{gas}}}{\pi\left(d_{\text{inlet}}^2/4\right)} \tag{15}$$

where the Q_{gas} is the carrier gas flow of the powder feeder, d_{inlet} is the diameter of the nozzle's inlet. The dynamic equations (Equations (10) and (11)) governing powder particles are addressed through the vertical injection of carrier gas at the inlet boundary, integrating the turbulent governing equations. The DPM module integrated within Fluent effectively implements the dynamic model of powder particles, which is coupled with the continuous medium gas model. The continuum model and discrete model are iteratively solved until convergence is achieved.

2.6. Powder Properties and Construction Materials

The Yttria-Stabilized Zirconia (YSZ) powder used in this study has a particle size distribution of 45–90 μm, following a Rosin-Rammler distribution. This powder is characterized by its high thermal stability and excellent performance under high-temperature conditions, making it suitable for the spheroidization process. The initial morphology of the powder particles is mostly spherical or quasi-spherical, with some irregular particles and surface imperfections. The chemical composition of the YSZ powder ensures consistent behavior during spheroidization.

The material feed device is constructed from brass and copper, chosen for their thermal properties and ability to withstand the operational conditions of the plasma torch. Brass provides excellent thermal conductivity and high-temperature resistance, ensuring uniform heat distribution and minimal thermal expansion. Copper offers high thermal conductivity and durability under high-temperature conditions, making it suitable for the nozzle tail and anode compression section.

2.7. Heat Exchange and Flow Dynamics

The annular powder feeding nozzle was optimized to enhance heat exchange and reduce friction. The nozzle's geometry and material selection ensure efficient heat transfer and minimal resistance to the flow of powder particles. The smooth inner surface of the nozzle minimizes friction, ensuring a consistent and uniform flow of powder particles.

The nozzle and reactor setup were optimized to ensure efficient flow dynamics within the reactor. The tangential powder feeding mechanism ensures a uniform distribution of powder particles, reducing the likelihood of unprocessed powder. The reactor setup, including the plasma jet characteristics and gas flow rates, was optimized to ensure adequate exposure of powder particles to the high-temperature plasma jet, minimizing unprocessed powder and improving spheroidization efficiency.

3. Experimental Details

3.1. Experimental Setup

The experimental setup, as shown in Figure 5, comprises seven key components: an annular powder-feeding plasma torch (APT), a DC power supply system, a double-loop cooling system, a rotary powder feeder, a gas supply system, a powder collection system, and a data acquisition system. This setup was specifically designed to assess the performance of the newly developed annular powder-feeding plasma torch in achieving uniform powder distribution, efficient spheroidization, and high-quality deposition.

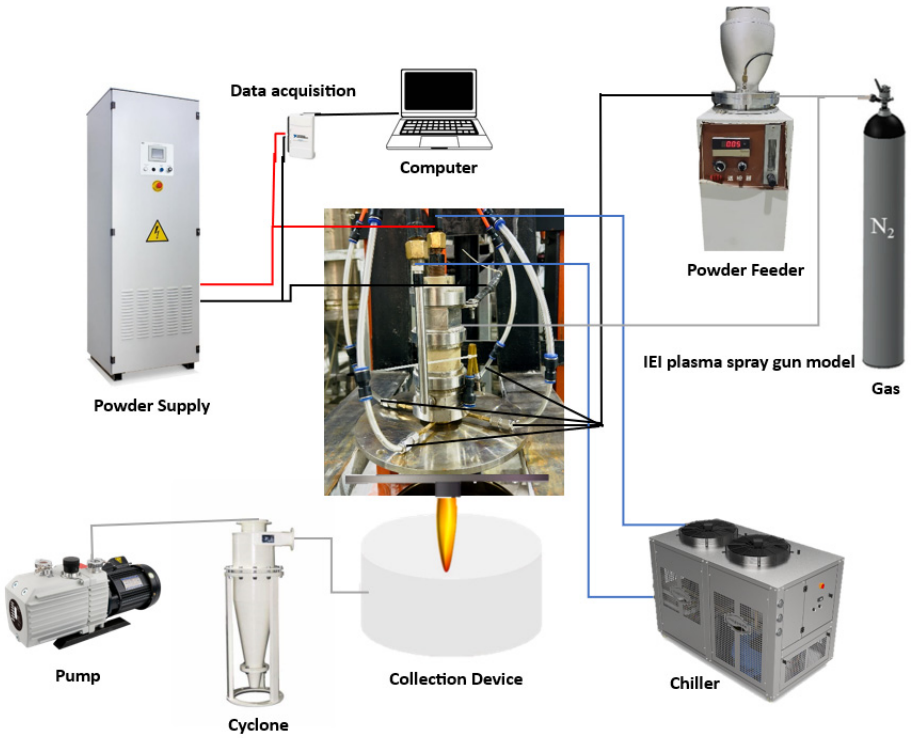

Figure 5. Schematic diagram of the experiment's setup using an annular powder-feeding plasma torch.

The plasma spheroidization system had a vertical plasma torch with an annular nozzle that included tangential powder feeding and cooling channels. This has allowed uniform powder distribution and reduced thermal stresses by providing long-term operations. The carrier gas was argon at flow rates of 5 to 17 L/min, and nitrogen was used as the plasma forming gas. A rotary powder feeder was used to supply the Yttria-Stabilized Zirconia (YSZ) powder, having a

particle size distribution between 45–90 μm according to a Rossin-Rammler distribution at feed rates from 1.5 to 3.0 r/min. All experiments were conducted with the plasma arc current held at 100 A to ensure stable operation.

3.2. Arc Discharge Parameters and Material Feed Device

The plasma torch operates at a maximum power of 30 kW, with the plasma arc current maintained at 100 A throughout the experiments. The plasma jet operates at temperatures exceeding 6000 K, ensuring complete melting of the powder particles. The electron concentration in the plasma jet is estimated to be in the range of 10^{15} to $10^{16}\mathrm{cm}^{-3}$, based on the operating conditions and plasma gas composition. The experiments are conducted at atmospheric pressure to ensure stable operation and consistent results.

The material feed device is constructed from brass and copper, chosen for their thermal conductivity and high-temperature resistance. The nozzle body and ring groove section are made from brass, ensuring uniform heat distribution and minimal thermal expansion. The nozzle tail and anode compression section are made from copper, offering high thermal conductivity and durability under high-temperature conditions.

3.3. Experimental Procedure

The substrate was placed 250 mm below the nozzle to maintain a fixed spraying distance, and the torch was mounted vertically. Uniform deposition coverage was achieved with a 2 mm spacing between consecutive passes of a 2 mm serpentine motion path on a programmable two-dimensional motion platform. To visualize and study powder deposition patterns, sandpaper substrates of 100 mm × 100 mm were used. High-speed cameras were also included in the experimental system to record the powder jet morphology and the interactions between the plasma jet and the powder flow. This setup enabled precise analysis of the powder transport dynamics and deposition characteristics.

Three experimental investigations were conducted: powder distribution, powder spheroidization, and deposition performance. Powder flow uniformity as it exits the annular nozzle was investigated using powder distribution tests. The powder jet morphology was recorded at high speed, while a polar coordinate technique allowed measuring and mapping the particle distribution over the nozzle outlet. YSZ powder was injected into the plasma jet at 10, 15, and 20 SLM flow rates as shown in the Table 2, besides the other parameter which used in the experiments, and the spheroidized powder was collected and analyzed via a Scanning Electron Microscope (SEM). The extent of spheroidization was assessed based on parameters such as circularity, surface roughness, and size uniformity. To better assess the spheroidization quality under different conditions, additional experiments were conducted using raw powder with non-spherical particles. These powders had a broader range of particle shapes and surface textures compared to the standard spherical YSZ powder. The non-spherical particles were introduced into the plasma jet under the same conditions as the spherical powder to evaluate their behavior during spheroidization.

Table 2. Experimental Parameters.

Parameter	Values	Unit
Gas Flow Rate (L/min)	5 to 17	L/min
Powder Feeding Rate (g/min)	1.5 to 3.0	g/min
Plasma Arc Current	100	A
Duration	10	min
Morphological Stability	Nitrogen: 10, 15, 20	SLM
Spheroidization	Nitrogen: 10, 15, 20	SLM

4. Results and Discussion

4.1. Powder Distribution and Uniformity

The performance of the novel annular powder feeding nozzle was rigorously evaluated to determine its capability for superior powder distribution uniformity compared to conventional nozzle designs. Utilizing a polar coordinate approach, the powder distribution patterns at the nozzle outlet were analyzed by dividing the circular outlet into 28 equal segments, each corresponding to an individual channel of the nozzle [44,45]. The results showed minimal deviation in particle count across the sampled segments, confirming highly uniform powder dispersion. This uniformity is critical for high-quality coatings, adhesion, and performance in plasma spraying applications.

A comparison of powder distribution and uniformity between the novel annular nozzle design and the traditional nozzle design is shown in Figure 6. The new design, with a circular outlet divided into 28 equal segments and 4 inlet

powder and gas lines, demonstrated uniform powder delivery and minimized dispersion. In contrast, the traditional nozzle, with a circular outlet divided into 32 equal segments and only 2 inlet lines, exhibited non-uniform powder distribution, leading to unstable jet performance. The powder capture efficiency and uniformity index of the new annular nozzle were evaluated. Traditional discrete outlet nozzles capture only 36% of the powder, whereas the optimized annular nozzle achieves a powder capture efficiency of 75%. This improvement is attributed to the annular geometry, which reduces turbulent flow and increases particle convergence, resulting in more efficient and uniform powder delivery.

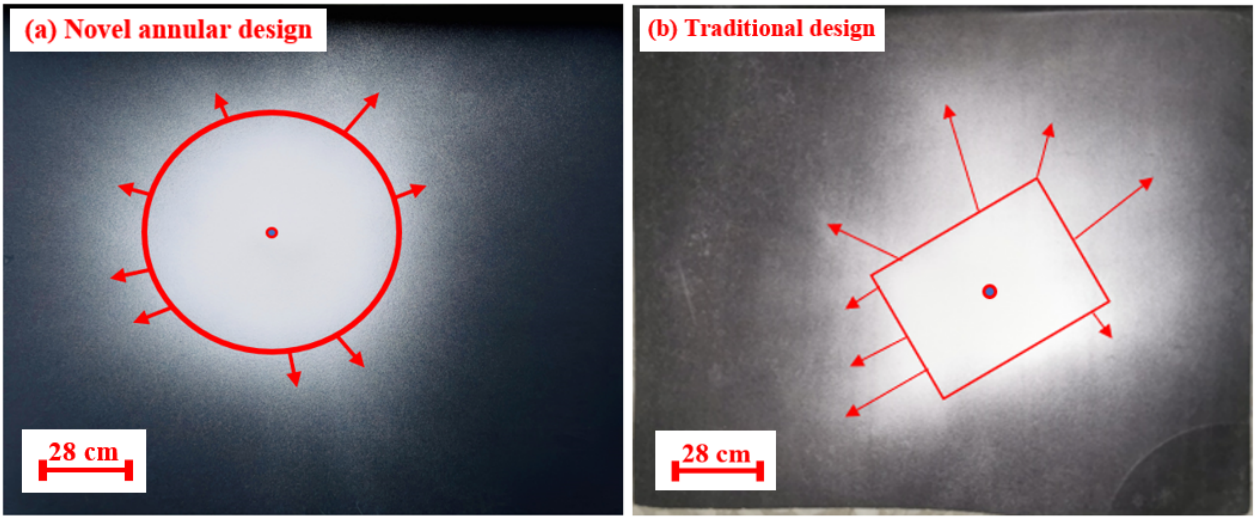

Figure 6. Comparison of Powder distribution and uniformity of (**a**) Novel annular design and (**b**) Traditional design.

Table 3. Comparison of Powder Capture Efficiency and Uniformity Index between Traditional and Annular Nozzles.

Nozzle Design	Powder Capture Efficiency (%)	Uniformity Index
Traditional Discrete-Outlets	36%	0.72
Proposed Annular Nozzle	75%	0.95

The uniformity index, a measure of the consistency of powder distribution, further supports these findings. The discrete-outlet nozzle had a uniformity index of 0.72, while the proposed annular nozzle had a significantly higher value of 0.95 as shown in the Table 3. The new design shows a substantial improvement in the uniformity index, indicating that the new design can maintain stable and symmetric powder delivery. The uniformity index is critical to producing coatings with reduced porosity, higher thermal and wear properties, thus making the annular nozzle suitable for industrial plasma spraying applications.

4.2. The Morphology and Structure of the Spherical Powder

To assess the spheroidization efficiency and particle quality of Yttria-Stabilized Zirconia (YSZ) under different gas flow rates of 10, 15, and 20 SLM, the morphology and structural characteristics of YSZ powder were rigorously investigated. The raw YSZ powder, examined by optical imaging (As shown in Figure 7a), displayed mostly spherical or quasi-spherical morphology with some irregular particles and surface imperfections. The existence of these irregularities indicates that spheroidization is incomplete and may affect the flowability and processing efficiency of the particle. The circularity index (CI) is used to quantify the spheroidization efficiency. The CI is calculated using the formula:

$$\mathrm{CI} = \frac{4\pi * Area}{Perimeter^2} \tag{16}$$

where the area and perimeter of each particle are measured from the SEM images. Particles with a CI greater than 0.9 are considered highly spherical. It shows in Figure 7b that the particle size distribution is wide, requiring the control of particle size and morphology in producing high-quality powder for powder processing.

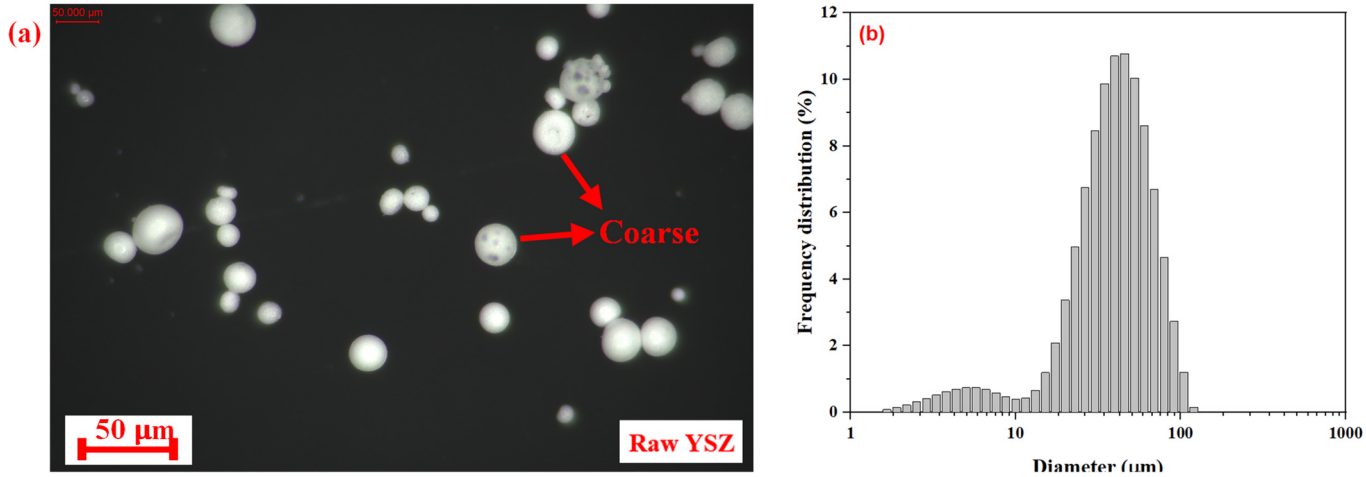

Figure 7. Optical images and particle size distribution of (**a**) raw powder, (**b**)

At 10 SLM, the optical and SEM images (As shown in Figures 8a,d and 9d–f) display particles with irregular shapes and rough surfaces, indicative of insufficient thermal energy transfer and incomplete melting. These particles had a circularity index below 0.85 and a spheroidization rate of about 70%. This is in agreement with previous studies that have demonstrated that lower gas flow rates lead to insufficient heating and, therefore, lower spheroidization efficiency. SEM analysis (As shown in Figure 9a–c) further confirms that the raw powder is predominantly spherical but contains porous structures that contribute to elevated gas content and thinner shell thickness. Three gas flow rates were tested: 10 SLM, 15 SLM, and 20 SLM. The spheroidization efficiency, a key parameter for optimization of powder characteristics, was evaluated at each flow rate.

At 15 SLM, significant improvements in particle morphology were observed, as evidenced by the SEM images (As shown in Figures 8b,e and 9g–i). The particles exhibited smoother, more spherical surfaces with a narrower and more uniform particle size distribution, indicating the achievement of optimal spheroidization conditions. The spheroidization rate increased to about 85%, and the circularity index was above 0.90. The improvements in particle morphology indicate that the gas flow rate of 15 SLM is the optimal thermal energy for uniform melting and shaping of the particles. This enhanced spheroidization at 15 SLM plays a direct role in more consistent powder flow, lower levels of agglomeration, and greater material efficiency, thereby improving general process efficiency.

At 20 SLM, the optical and SEM images (As shown in Figures 8c,f and 9j–l) show a slight degradation in particle morphology, with some surface irregularities and a decrease in circularity. These observations indicate that the overheating was caused by excessive gas flow, which resulted in less controlled particle formation. In the transition regime, the spheroidization rate was about 75%, and the circularity index was 0.85, demonstrating the negative effect of excessive turbulence and defocusing on particle size control. At this flow rate, it is further verified that the excessive gas flow alters particle formation uniformity.

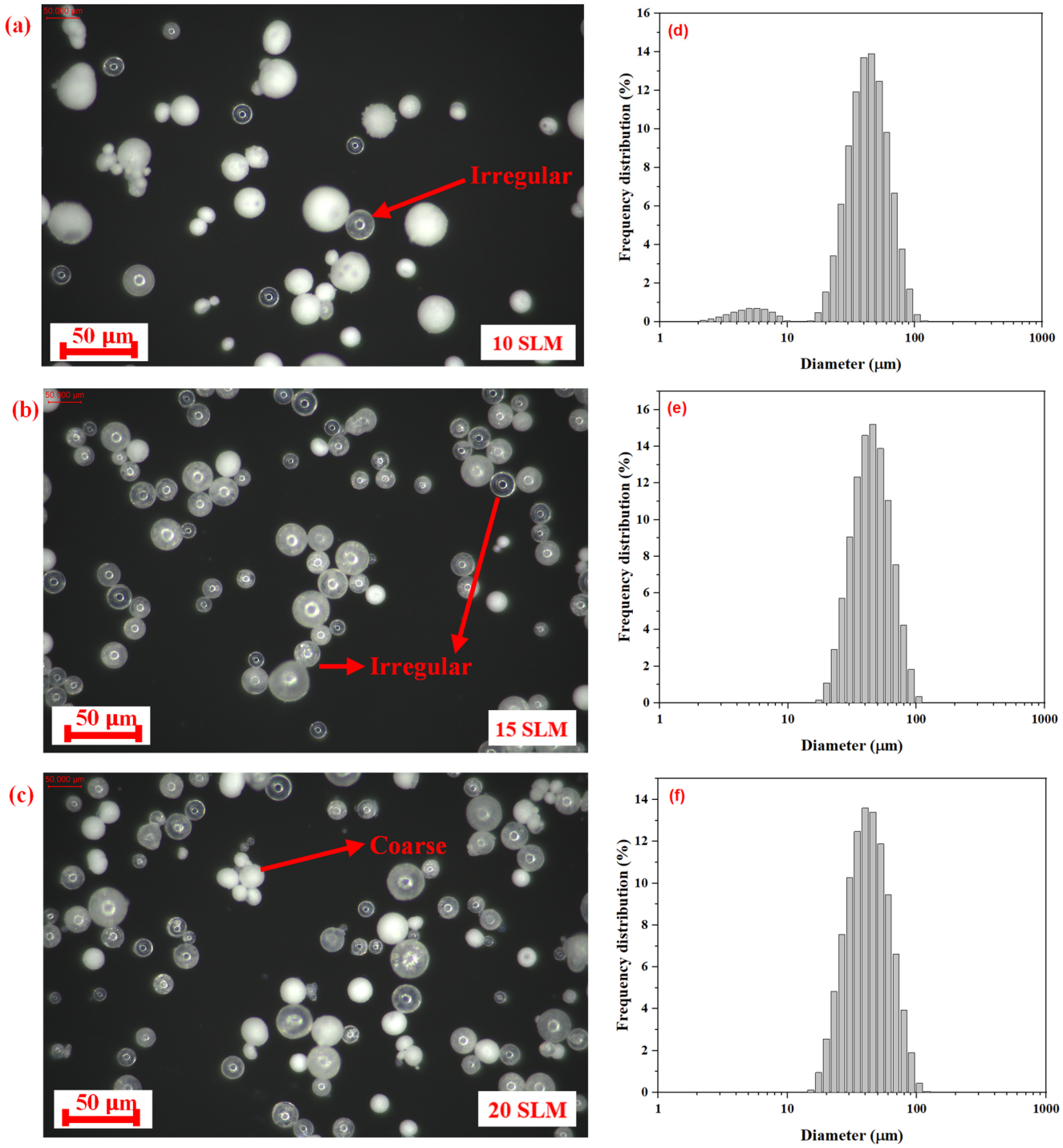

Figure 8. Optical images and particle size distribution of (**a**,**d**) 10 SLM, (**b**,**e**) 15 SLM, (**c**,**f**) 20 SLM.

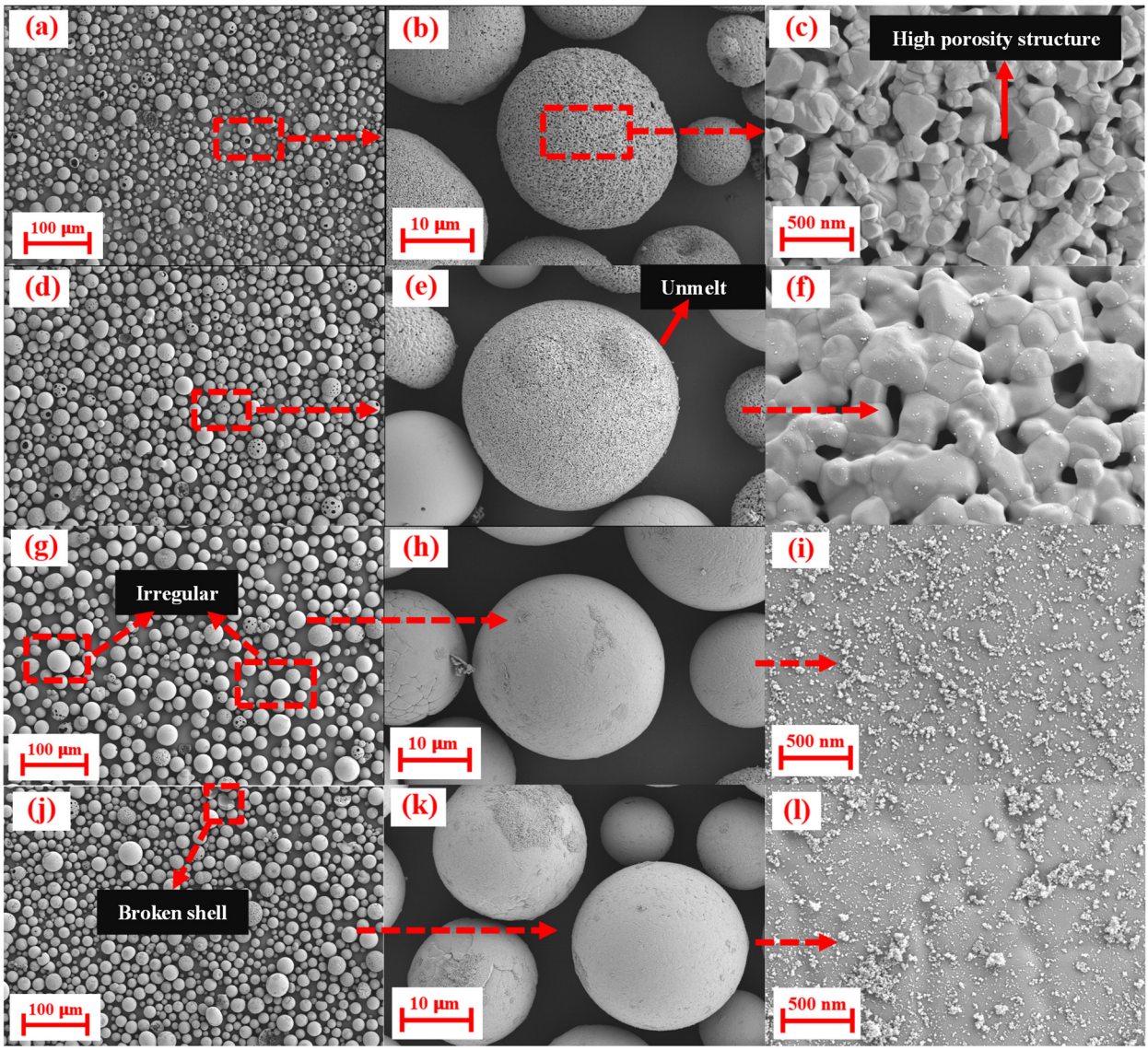

Figure 9. SEM images of powder: (**a**–**c**) raw powder, (**d**–**f**) used 10 SLM, (**g**–**i**) used 15 SLM, (**j**–**l**) used 20 SLM.

Additional experiments using non-spherical powder showed varied results in spheroidization quality. While some irregularly shaped particles exhibited reduced spheroidization efficiency compared to spherical particles, the annular nozzle design still demonstrated superior performance, achieving a spheroidization rate of approximately 70% for non-spherical particles. The results suggest that the nozzle's uniform powder distribution plays a crucial role in mitigating the negative effects of particle shape on spheroidization.

The results show that the novel annular powder-feeding plasma torch outperforms traditional nozzle configurations. The annular geometry demonstrated higher powder capture efficiency (75%) compared to traditional discrete-outlet nozzles (36%). The annular nozzle also showed a 92% deposition efficiency, compared to 75% for conventional nozzles and 85% for coaxial nozzles as shown in Table 4. These results indicate that the annular design is more efficient in terms of powder capture and deposition, which can be directly attributed to the optimized flow dynamics and powder-gas interaction of the design.

Table 4. Calculation of Spheroidization Rates.

Gas Flow Rate (SLM)	Circularity Index	Spheroidization Rate (%)
10	<0.85	~70%
15	>0.90	~85%
20	~0.85	~75%

The increased spheroidization efficiency with the annular nozzle is attributed to its uniform and symmetric powder distribution, which maximizes thermal energy transfer to the particles. The tangential powder feeding mechanism

provided by the annular nozzle ensures uniform delivery of powder into the plasma stream, minimizing defocusing and agglomeration. The spheroidization rate reached 85% at a gas flow rate of 15 SLM, with a circularity index above 0.90, indicating highly spherical particles with optimized morphology. The results show that the annular nozzle improves the efficiency and quality of powder spheroidization and reduces material waste during the process. At 15 SLM, the narrow and uniform particle size distribution, along with a high circularity index, implies superior performance of the new design. The annular nozzle enhances powder utilization efficiency, with particles being more uniformly heated and achieving better overall process performance. The advantages of the annular powder-feeding plasma torch make it a much more effective solution than traditional systems, resulting in better spheroidization with less material loss.

4.3. The Comparison of Annular Powder-Feeding and Radial Powder Feeding

In this study, we compared two different nozzle designs as shown in the Figure 10: the novel annular powder-feeding nozzle and the traditional powder-feeding nozzle. The novel annular nozzle features four tangential inlet lines and 28 grooves, which provide uniform and symmetrical powder distribution. In contrast, the traditional nozzle design includes two tangential inlet powder lines and 32 grooves, resulting in less uniform powder distribution.

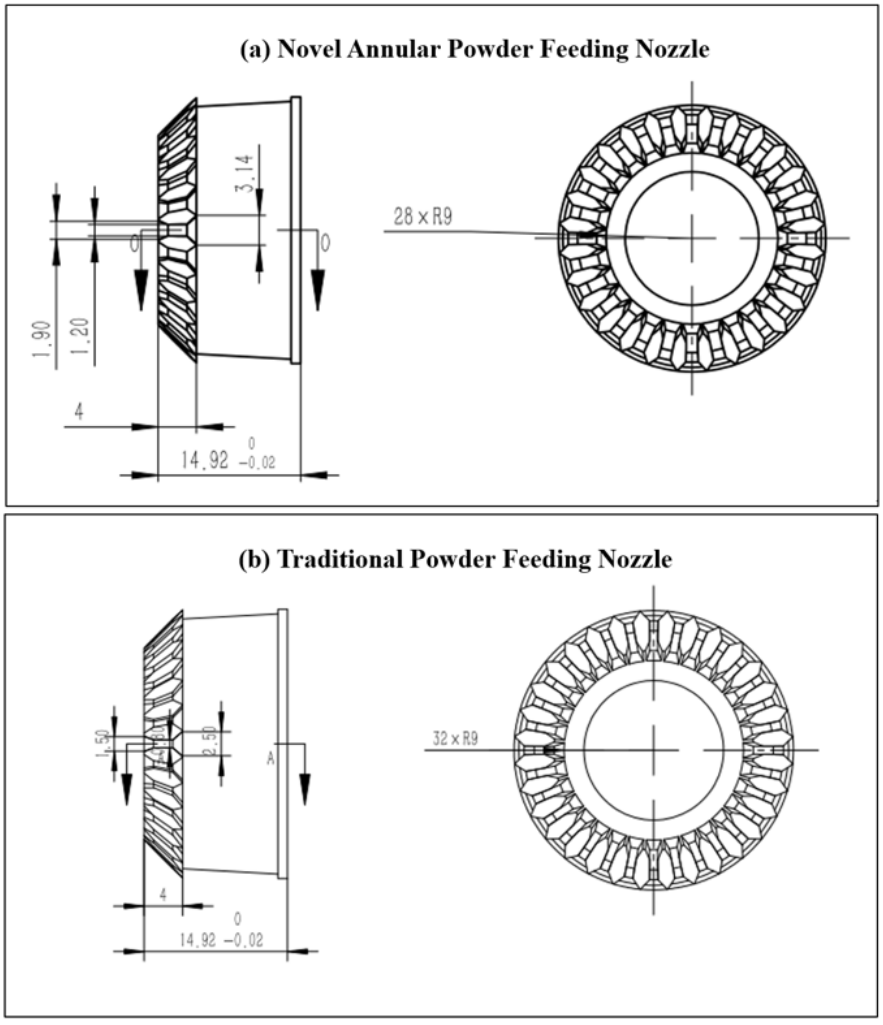

Figure 10. Schematics of the Nozzle Designs; (**a**) Novel Annular Powder Feeding Nozzle, and (**b**) Traditional Powder Feeding Nozzle.

As shown in Table 5, the novel annular nozzle (4 tangential inlets, 28 grooves) provides uniform powder distribution, achieving 85% spheroidization efficiency (85% particles > 0.9 circularity) and 92% deposition efficiency. In contrast, the traditional nozzle (2 inlets, 32 grooves) exhibits non-uniform distribution, with lower efficiencies (70% spheroidization, 75% deposition). The novel design demonstrates superior performance in powder uniformity and process efficiency. The ability of the novel annular powder-feeding nozzle to provide better distribution uniformity than the traditional powder-feeding nozzle design was rigorously evaluated. As shown in Figure 11, the orthogonal mass assessment indicates that the mesh quality of the novel nozzle design is above the critical threshold of 0.1, guaranteeing

the stability and accuracy of the simulations and demonstrating the successful application of the mesh refinement process to the ring groove section. In practical applications, improved mesh quality is essential for the reliable performance of the nozzle.

Table 5. Comparative Characteristics of Nozzle Designs.

Nozzle Design	Inlet Lines	Grooves	Powder Distribution	Spheroidization Efficiency	Deposition Efficiency
Novel Annular	4 Tangential	28	Uniform & Symmetrical	85% (85% particles > 0.9 circularity)	92%
Traditional	2 Tangential	32	Non-uniform	70% (70% particles > 0.9 circularity)	75%

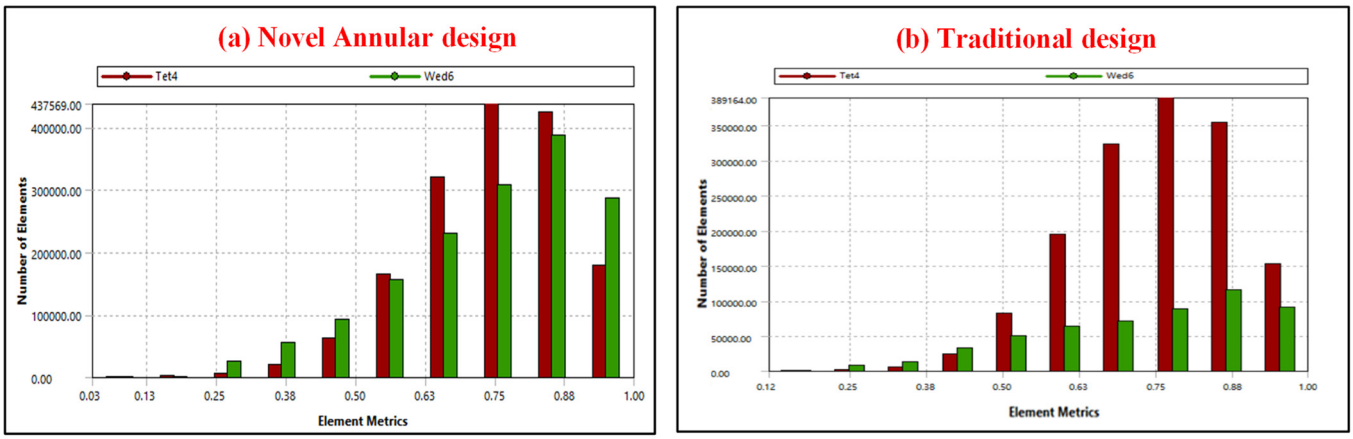

Figure 11. (**a**) Powder Distribution Uniformity Comparison between Novel Annular and (**b**) Traditional Nozzles.

Comparing the two powder distribution designs, the new annular powder-feeding nozzle shows a much better improvement in uniformity than the traditional nozzle. As shown in Figure 11a, the annular design with four inlet powder lines and 28 grooves provides a much more uniform powder flow over the entire print area. This design optimality results in a uniform distribution of material minimizes disturbances in the plasma flow, and increases the interaction of the particles with the plasma jet. Reducing flow disturbances makes the powder output more consistent and controlled, which is crucial for high-quality processing outcomes and the reduction of material waste. In contrast, Figure 11b shows the powder distribution of the traditional nozzle with two inlet powder lines and 32 grooves. In the traditional design, the powder is non-uniformly distributed across the surface of the nozzle, with some areas having more powder while others are underfed. Poor deposition control, material loss, and inefficient powder utilization due to this non-uniformity can affect the overall process stability. The limited inlet and groove design of the traditional nozzle is unable to provide uniform powder distribution, which is due to the lack of precision and control that the annular design provides.

The number and configuration of inlet lines and the groove design are the key differences between the novel annular powder-feeding nozzle and the traditional design. The four inlet lines and 28 grooves of the novel annular nozzle allow for a more balanced and symmetrical distribution of powder, leading to a more even flow of powder through the nozzle. In contrast, the traditional nozzle, with more grooves (32), is less effective because there are fewer inlet lines, resulting in less controlled powder flow. In addition, the annular nozzle is designed such that the powder is fed more equally into the plasma jet with little deflection or agglomeration of particles. This improved powder-feeding efficiency decreases the chance of powder loss and leads to more efficient spheroidization and processing. With less efficient powder flow dynamics from the traditional nozzle, the amount of control to achieve the same level of uniformity is lost, leading to less consistent powder output and decreased efficiency in powder utilization.

Discrete Phase Modeling (DPM) was used to analyze powder particle trajectories and distribution performance through the evaluation of different designs for annular powder-feeding nozzles. Two nozzle configurations were studied: the novel annular nozzle and the traditional nozzle. As shown in Figure 12, the results show that the ring groove annular powder-feeding nozzle can achieve a much more uniform distribution of powder-feeding efficiency and plasma jet stability compared to the traditional design.

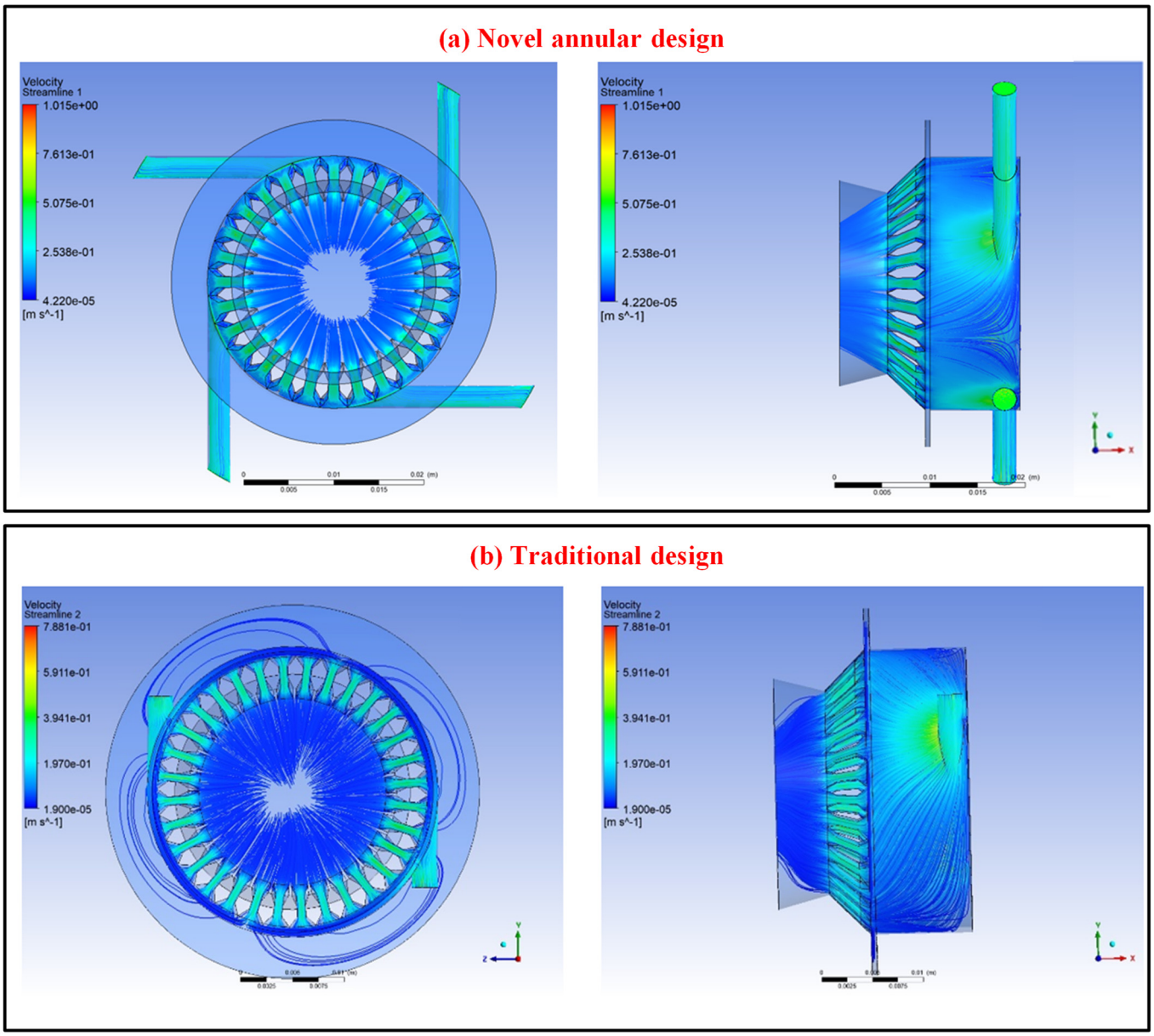

Figure 12. Simulation Results of Powder Distribution for (**a**) Novel and (**b**) Traditional Annular Powder-Feeding Nozzle Designs (Ring Groove and Slit Nozzles)—Bottom and Side Views.

The bottom-view simulation results of the novel annular nozzle with the ring-groove design are shown in Figure 12a. Particle density is highest near the feed ports and decreases as particles move further from the nozzle. Even though the density of powder drops with distance from the inlet, the design of the manifold manages to redistribute the powder such that an axisymmetric powder distribution is approximately obtained at the outlet. Consistent material deposition and good process stability are realized only when the powder is distributed uniformly. It also shows the side view analysis that confirms that the manifold design evenly splits each incident powder stream into two opposing streams for more controlled and uniform powder delivery. These improved symmetry and consistency of powder feeding result in improved powder feeding efficiency, minimized powder loss, and better deposition quality.

Figure 12b shows the simulation results for the traditional nozzle. The balanced dual powder feed ports result in a symmetric powder distribution at the outlet of this nozzle design. However, the powder distribution is still non-uniform, with higher concentrations at opposite ends of the nozzle and lower concentrations in between. The side-view trajectory analysis shows that, even with the feed ports that mitigate some of the disturbance, particles travel in different directions and form an asymmetric deposition pattern. The non-uniformity of the powder negatively impacts powder feeding efficiency and process stability. The novel annular powder-feeding nozzle with the manifold ring-grooved design Figure 12a shows much better powder distribution uniformity, powder-feeding efficiency, and plasma jet stability than the traditional design Figure 12b. More efficient powder feeding, lower risk of powder loss, and better deposition and spheroidization are achieved in the novel axisymmetric design by optimization of enhanced axisymmetric powder

distribution and control of particle flow. The optimized powder delivery is a key factor in enhancing the overall performance of powder-feeding systems, which verifies that the novel annular powder-feeding nozzle is much more efficient than the traditional powder-feeding nozzle designs.

The results of this simulation highlight the merits of the new annular powder-feeding nozzle with superior powder distribution uniformity and better efficiency than most conventional powder-feeding arrangements. Precise and reliable feeding requires that the powder delivery be as consistent as possible. This novel design, with performance and stability, greatly outperforms currently used powder feeders in practical applications.

The performance of the novel annular powder-feeding nozzle design was analyzed through simulation results as well as statistically analyzing powder distribution and compared with the traditional nozzle configurations. Figure 13a shows that the newly designed annular powder-feeding nozzle with an integrated ring groove has a highly uniform and symmetrical powder distribution at the nozzle outlet. The simulation results agree very well with the statistics, confirming that the model is robust and accurate. Typical of an effective powder delivery system, the particle concentration is highest near the powder inlet and decreases as particles move away from the nozzle. The most notable feature is the symmetrical distribution of powder across the entire outlet, which guarantees uniform material deposition. The results clearly show that the novel annular powder-feeding nozzle offers much better powder distribution uniformity than conventional designs.

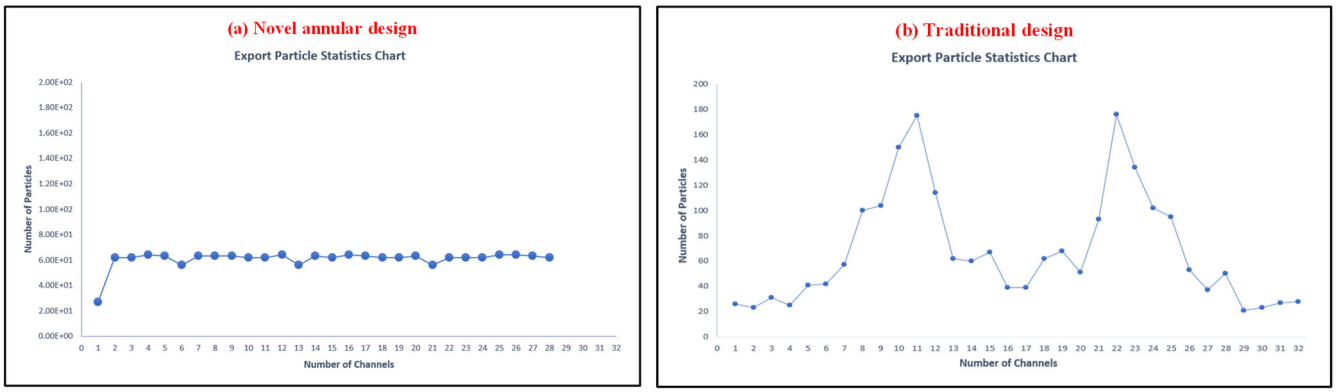

Figure 13. Powder Distribution for Different Nozzle Designs. (**a**) Novel Annular Groove Nozzle, Showing Uniform and Symmetrical Flow. (**b**) Traditional Nozzle, Exhibiting Asymmetrical Distribution.

In contrast, Figure 13b shows the powder distribution for the traditional nozzle design. The general trend of particle concentration is similar to the novel design, but the distribution pattern is less uniform and does not have the clear symmetry of the new design. The powder distribution in the traditional nozzle is non-uniform, which indicates that the powder feeding mechanism is less efficient. Due to this irregular distribution, the material deposition might not be consistent, leading to operation challenges such as varying material flow rates, uneven coverage, or material waste. Such implications demonstrate that the drawbacks that arise from the inherent limitations of the traditional nozzle designs in offering stable and uniform powder delivery are not exaggerated. Furthermore, the statistical alignment with the simulation data, along with the powder distribution symmetry, confirms the superior performance of the novel annular powder-feeding nozzle. These results prove that the new design is much more capable of providing uniform powder delivery, which results in improved process control and lower inefficiencies present in traditional designs. The novel design of the powder disperser provides a method of consistent powder distribution. It ensures low levels of issues in maintaining solid conditions in the bowl, which is ideal for use in high-precision applications.

The single-inlet ring groove nozzle design was further investigated, as shown in Figure 14. This figure presents the statistical results, which are in strong correlation with the simulation data, thereby confirming the reliability of the findings. The powder concentration is highest near the inlet, as expected from the flow dynamics, and decreases gradually as the powder travels downstream. The resulting symmetrical distribution verifies the efficient and consistent powder distribution characteristics of the single-inlet ring groove nozzle, which is crucial for stable and reliable powder delivery. The uniform powder distribution pattern indicates that the nozzle effectively reduces issues such as clogging, uneven feeding, and material wastage.

The experimental results show that the annular groove and single-inlet ring groove nozzle designs provide a more uniform powder distribution compared to conventional nozzle configurations. The data, supported by both simulation and experimental results, demonstrate that these designs lead to more stable operation, reduced material waste, and

enhanced process efficiency. The annular powder-feeding nozzle's uniform powder distribution and controlled feeding mechanism make it effective for applications requiring precise powder delivery, as shown in Figures 6 and 13.

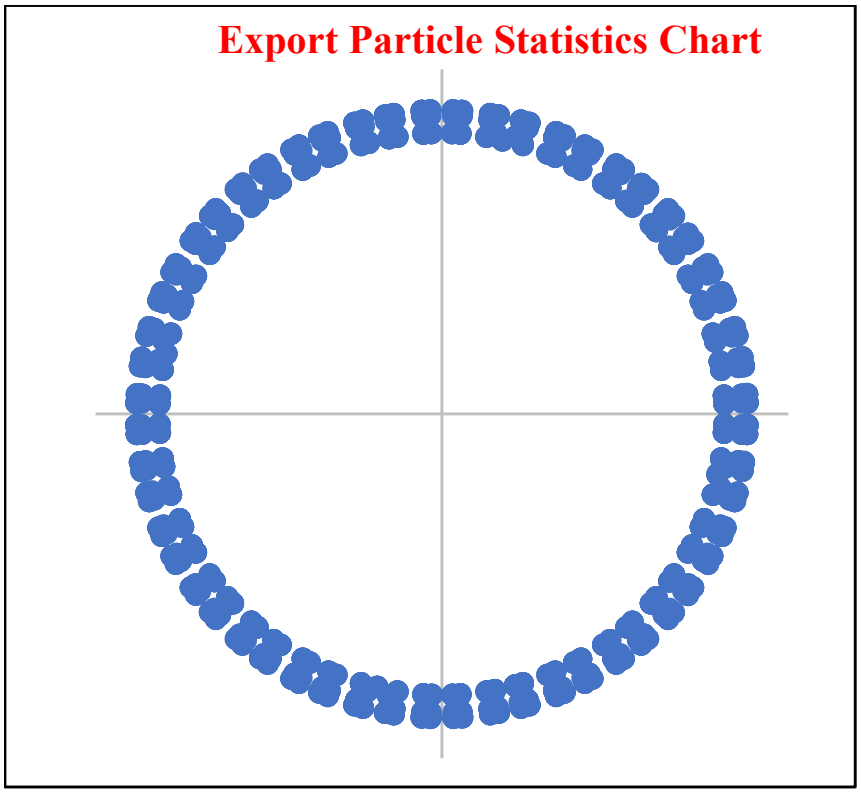

Figure 14. Powder Distribution of the Single-Inlet Ring Groove Nozzle, Demonstrating a Symmetrical and Uniform Flow Pattern.

5. Conclusions

To evaluate the performance of a novel annular powder feeding nozzle, a three-dimensional numerical model of gas-powder two-phase flow has been developed. The momentum transfer between gas and powder particles is described using the two-way turbulence coupling method, and the powder movement dynamics during the feeding process are analyzed. The key findings are:

(1) Superior Powder Capture and Deposition Efficiency: The novel annular nozzle achieved a powder capture efficiency of 75% and a deposition efficiency of 92%, significantly higher than traditional (36% capture, 75% deposition) and coaxial (60% capture, 85% deposition) nozzles. This improvement is attributed to the optimized annular geometry and tangential powder feeding mechanism, which ensures a more uniform powder distribution.

(2) Enhanced Spheroidization Quality: Over 85% of the particles from the annular nozzle had a circularity index greater than 0.9, compared to 70% and 80% for traditional and coaxial nozzles, respectively. This enhanced quality ensures more consistent particle behavior and effective deposition, which is crucial for applications requiring precise material delivery and uniformity.

(3) Improved Process Stability: The uniform powder distribution reduces the risk of operational issues such as uneven powder delivery and clogging. Adjusting the gas flow rate or reducing the powder feed rate can mitigate potential blockages, ensuring stable powder flow and efficient material utilization.

Author Contributions

M.S.I.: Formal analysis, Project administration, Data curation, Conceptualization, Methodology, Writing—original draft; D.Y.: Formal analysis, Funding acquisition, Project administration, Writing—Review & Editing; J.Q.: Formal analysis, Investigation; Y.X.: Supervision, Validation; Y.F.: Supervision, Investigation.

Ethics Statement

Not applicable.

Informed Consent Statement

Not applicable.

Data Availability Statement

The data that support the findings of this study are available from the corresponding author upon reasonable request.

Funding

This research was funded by [the National Natural Science Foundation of China] grant number [52274364] and [the Sichuan Science and Technology Program] grant number [2024ZDZX0039].

Declaration of Competing Interest

The authors declared that they have no conflicts of interest to this work. We declare that we do not have any commercial or associative interest that represents a conflict of interest in connection with the work submitted.

References

1. Dobrzański L, Dobrzański L, Dobrzańska-Danikiewicz A, Kraszewska M. Manufacturing powders of metals, their alloys and ceramics and the importance of conventional and additive technologies for products manufacturing in Industry 4.0 stage. *Arch. Mater. Sci. Eng.* **2020**, *102*. doi:10.5604/01.3001.0014.1452.
2. Chaturvedi V, Ananthapadmanabhan P, Chakravarthy Y, Bhandari S, Tiwari N, Pragatheeswaran A, et al. Thermal plasma spheroidization of aluminum oxide and characterization of the spheroidized alumina powder. *Ceram. Int.* **2014**, *40*, 8273–8279.
3. Uskoković D, Uskoković V. Magical spherical particles produced by centrifugal atomization. *Powder Technol.* **2024**, *444*, 120017.
4. Shanmugavelayutham G, Selvarajan V. Plasma spheroidization of nickel powders in a plasma reactor. *Bull. Mater. Sci.* **2004**, *27*, 453–457.
5. Wei W, Wang L, Chen T, Duan X, Li W. Study on the flow properties of Ti-6Al-4V powders prepared by radio-frequency plasma spheroidization. *Adv. Powder Technol.* **2017**, *28*, 2431–2437.
6. Boulos M. Plasma power can make better powders. *Met. Powder Rep.* **2004**, *59*, 16–21.
7. Wang K, Tong Y, Chen Y, Kong L, Lu K, Wang J, et al. Powder stream performance of a novel annular laser direct metal deposition with inside-laser coaxial powder feeding nozzle: Simulation and experimental perspectives. *Opt. Laser Technol.* **2024**, *175*, 110723.
8. Khamidullin B, Tsivilskiy I, Gorunov A, Gilmutdinov AK. Modeling of the effect of powder parameters on laser cladding using coaxial nozzle. *Surf. Coat. Technol.* **2019**, *364*, 430–443.
9. Sun Q, Zhi G, Zhou S, Dong X, Shen Q, Tao R, et al. Advanced Design and Manufacturing Approaches for Structures with Enhanced Thermal Management Performance: A Review. *Adv. Mater. Technol.* **2024**, *9*, 2400263.
10. López-Martínez A, Ibarra-Medina J, García-Moreno A, Piedra S, del Llano Vizcaya L, Martínez-Franco E, et al. Modeling and comparison of the powder flow dynamics for tilted annular and discrete-outlet nozzles in laser directed energy deposition. *J. Manuf. Process.* **2023**, *99*, 687–704.
11. Yadegari MJ, Martucci A, Biamino S, Ugues D, Montanaro L, Fino P, et al. Aluminum Laser Additive Manufacturing: A Review on Challenges and Opportunities Through the Lens of Sustainability. *Appl. Sci.* **2025**, *15*, 2221.
12. Liu Y, Li Y, Wang M, Chen Z. Review of Laser Powder Bed Fusion's Microstructure and Mechanical Characteristics for Al-Ce Alloys. *Materials* **2024**, *17*, 5085.
13. Goh GD, Wong KK, Tan N, Seet HL, Nai MLS. Large-format additive manufacturing of polymers: A review of fabrication processes, materials, and design. *Virtual Phys. Prototyp.* **2024**, *19*, e2336160.
14. Hou PC-H. Development of a Micro-Feeder for Cohesive Pharmaceutical Powders. PhD thesis, University of Strathclyde, Glasgow, Scotland, 2024.
15. Luo S, Feng Y, Song J, Xu D, Xia K. Progress and challenges in exploration of powder fueled ramjets. *Appl. Ther. Eng.* **2022**, *213*, 118776.
16. Guner A, Bidare P, Jiménez A, Dimov S, Essa K. Nozzle designs in powder-based direct laser deposition: a review. *Int. J. Precis. Eng. Manuf.* **2022**, *23*, 1077–1094.
17. Russell A, Strong J, Garner S, Ketterhagen W, Long M, Capece M. Direct compaction drug product process modeling. *AAPS PharmSciTech* **2022**, *23*, 67.
18. Samokhin A, Alekseev N, Sinayskiy M, Astashov A, Kirpichev D, Fadeev A, et al. Nanopowders production and micron-sized powders spheroidization in DC plasma reactors. *Powder Technol.* **2018**, *1*, 1–18.

19. Sista KS, Moon AP, Sinha GR, Pirjade BM, Dwarapudi S. Spherical metal powders through RF plasma spherodization. *Powder Technol.* **2022**, *400*, 117225.
20. Kumar S, Selvarajan V, Padmanabhan P, Sreekumar K. Spheroidization of metal and ceramic powders in thermal plasma jet: Comparison between experimental results and theoretical estimation. *J. Mater. Process. Technol.* **2006**, *176*, 87–94.
21. Bao Q, Yang Y, Wen X, Guo L, Guo Z. The preparation of spherical metal powders using the high-temperature remelting spheroidization technology. *Mater. Des.* **2021**, *199*, 109382.
22. Fan Y, Yu D, Qiu J, Xiao Y, Qu Y, Gao Z, et al. Development and Performance Analysis of a Novel Triple-Anode Plasma Torch with Annular Powder Feeding for High-Efficiency Powder Processing. 2024. Available online: https://www.researchsquare.com/article/rs-5296634/v1 (accessed on 1 September 2024).
23. Zhang Z, Wang C, Sun Q, Zhu S, Xia W. Spheroidization of tungsten powder by a DC arc plasma generator with multiple cathodes. *Plasma Chem. Plasma Process.* **2022**, *42*, 939–956.
24. Boulos MI, Fauchais PL, Pfender E. Plasma–Particle Interactions in Thermal Plasma Processing. In *Handbook of Thermal Plasmas*; Boulos MI, Fauchais PL, Pfender E, Eds.; Springer International Publishing: Cham, Switzerland, 2023; pp. 1217–1309.
25. Qiu J, Yu D, Xiao Y, Fan Y, Chen Y, Li D. A novel triple-cathode plasma torch with hot-wall nozzle for YSZ spherical thin-walled hollow-shell powder preparation. *Ceram. Int.* **2023**, *49*, 27551–27566.
26. Boulos MI, Fauchais PL, Pfender E. Plasma Spray Torches. In *Handbook of Thermal Plasmas*; Boulos MI, Fauchais PL, Pfender E, Eds.; Springer International Publishing: Cham, Switzerland, 2023; pp. 795–848.
27. Murphy AB. Handbook of Thermal Plasmas, M. I. Boulos, P. L. Fauchais and E. Pfender (Eds). Springer Nature (Cham, 2023): Hardcover, 1975 pages, ISBN: 978-3-030-84934-4, Ebook: ISBN 978-3-030-84935-1, Living reference work: ISBN 978-3-030-84936-8. *Plasma Chem. Plasma Process.* **2023**, *43*, 1277–1279. doi:10.1007/s11090-023-10367-2.
28. Yang Z, Xu T, Li H, She M, Chen J, Wang Z, et al. Zero-dimensional carbon nanomaterials for fluorescent sensing and imaging. *Chem. Rev.* **2023**, *123*, 11047–11136.
29. den Hoed FM, Carlotti M, Palagi S, Raffa P, Mattoli V. Evolution of the microrobots: Stimuli-responsive materials and additive manufacturing technologies turn small structures into microscale robots. *Micromachines* **2024**, *15*, 275.
30. Wu X. Investigation of Metal to Composite Joining by Generative Rivets Technology. PhD Thesis, Brunel University, London, UK, 2024.
31. Kumar R, Rezapourian M, Rahmani R, Maurya HS, Kamboj N, Hussainova I. Bioinspired and multifunctional tribological materials for sliding, erosive, machining, and energy-absorbing conditions: A review. *Biomimetics* **2024**, *9*, 209.
32. Han Y-C, Zheng C, Liu Y-H, Wu X-L, Bian R-P, Liu P. Thermal characteristics and removal mechanism of high energy plasma jet rock-breaking. *Pet. Sci.* **2025**, *22*, 835–849.
33. Gaitonde D, Samimy M. Coherent structures in plasma-actuator controlled supersonic jets: Axisymmetric and mixed azimuthal modes. *Phys. Fluids* **2011**, *23*, 095104.
34. Nunes LDM. Computational Fluid Dynamics Application for Gas-Powder Flow Investigation in a Coaxial Nozzle Design for Additive Manufacturing. Master Thesis, Universidade Federal de Uberlândia, Uberlândia, Brasil, 2022.
35. Zhou H, Yang Y, Wang D, Li Y, Zhang S, Tai Z. Powder flow simulation of a ring-type coaxial nozzle and cladding experiment in laser metal deposition. *Int. J. Adv. Manuf. Technol.* **2022**, *120*, 8389–8400.
36. Naimanova A, Beketaeva A. A new non-equilibrium modification of the k− ω k-ω turbulence model for supersonic turbulent flows with transverse jet. *Int. J. Numer. Methods Fluids* **2025**, *97*, 69–87.
37. Nogdhe Y, Rai AK, Manjaiah M. Numerical study of powder flow characteristics of coaxial nozzle direct energy deposition at different operating and design conditions. *Prog. Addit. Manuf.* **2025**, *10*, 701–723.
38. Guan X, Zhao YF. Numerical modeling of coaxial powder stream in laser-powder-based Directed Energy Deposition process. *Addit. Manuf.* **2020**, *34*, 101226.
39. Shih T, Liou WW, Shabbir A, Yang Z, Zhu J. A new k-ϵ eddy viscosity model for high reynolds number turbulent flows. *Comput. Fluids* **1995**, *24*, 227–238.
40. Pereira O, Rodríguez A, Barreiro J, Fernández-Abia AI, de Lacalle LNL. Nozzle design for combined use of MQL and cryogenic gas in machining. *Int. J. Precis. Eng. Manuf.-Green Technol.* **2017**, *4*, 87–95.
41. Jayawickrama TR, Haugen NEL, Babler MU, Chishty MA, Umeki K. The effect of Stefan flow on the drag coefficient of spherical particles in a gas flow. *Int. J. Multiph. Flow.* **2019**, *117*, 130–137.
42. Morsi S, Alexander A. An investigation of particle trajectories in two-phase flow systems. *J. Fluid Mech.* **1972**, *55*, 193–208.
43. Lau TC, Nathan GJ. The effect of Stokes number on particle velocity and concentration distributions in a well-characterised, turbulent, co-flowing two-phase jet. *J. Fluid Mech.* **2016**, *809*, 72–110.
44. Thomas B. In-Situ Monitoring of Powder Flow in Directed Energy Deposition Additive Manufacturing. Master Thesis, The Pennsylvania State University, University Park, PA, USA, 2021.
45. Wu H, Xie X, Liu M, Chen C, Liao H, Zhang Y, et al. A new approach to simulate coating thickness in cold spray. *Surf. Coat. Technol.* **2020**, *382*, 125151.